NANOMATERIALS

Single-walled zeolitic nanotubes

Akshay Korde¹, Byunghyun Min¹, Elina Kapaca², Omar Knio¹, Iman Nezam¹, Ziyuan Wang¹, Johannes Leisen³, Xinyang Yin⁴, Xueyi Zhang⁴, David S. Sholl¹, Xiaodong Zou², Tom Willhammar^{2*}, Christopher W. Jones^{1,3*}, Sankar Nair^{1*}

We report the synthesis and structure of single-walled aluminosilicate nanotubes with microporous zeolitic walls. This quasi-one-dimensional zeolite is assembled by a bolaform structure-directing agent (SDA) containing a central biphenyl group connected by C_{10} alkyl chains to quinuclidinium end groups. High-resolution electron microscopy and diffraction, along with other supporting methods, revealed a unique wall structure that is a hybrid of characteristic building layers from two zeolite structure types, beta and MFI. This hybrid structure arises from minimization of strain energy during the formation of a curved nanotube wall. Nanotube formation involves the early appearance of a mesostructure due to self-assembly of the SDA molecules. The biphenyl core groups of the SDA molecules show evidence of π stacking, whereas the peripheral quinuclidinium groups direct the microporous wall structure.

eolites are widely used as size- and shapeselective catalysts and adsorbents because of their ordered microporous structure (1-3). There has been considerable interest in the synthesis of zeolites with hierarchical porosity (4-16) that allow access to a wider range of molecules. Early approaches (10-12) included postsynthesis treatments to etch mesopores into zeolite crystals. More recently, new structure-directing agents (SDAs) have been used to create two-dimensional (2D) zeolite nanosheets interspersed by mesoporous regions (6-8, 13-15), yielding nanosheets of several zeolitic topologies such as MFI, MWW, FAU, AEL, and others (6-13, 15-23). This is usually achieved with di-quaternary ammonium surfactant SDAs, in which the quaternary ammonium groups direct zeolite formation in two dimensions, whereas the long hydrocarbon moieties prevent zeolite crystallization in the third dimension. Interactions such as π stacking between the SDA molecules (15, 18-23) can also enhance their self-assembly into lamellar structures that allow 2D zeolite formation.

We report the first synthesis and structural characterization of a quasi-1D hierarchical zeolite, specifically a single-walled nanotube that has a microporous zeolitic wall enclosing a central mesoporous channel. We synthesized a bolaform SDA (BCPh10Qui; Fig. 1) that is capable of π stacking because of the central biphenyl moiety and has bulky quinuclidinium SDA head groups linked to the biphenyl moiety by C_{10} alkyl chains. This SDA was used for hydrothermal synthesis at 423 K in an alkaline

aluminosilicate medium with an Si/Al ratio of ~30 (see the supplementary materials, including fig. S1, for SDA and zeolite synthesis and characterization methods). Although "rational" design of SDAs for zeolite synthesis remains difficult and unreliable, we speculated that a long-chain SDA containing an aromatic $(\pi$ -stacking) species at its center might also template a nanotubular zeolite because many conventional surfactants can form lamellar and rodlike micelles. Further, the attachment of bulky quaternary ammonium head groups using sufficiently long and flexible alkyl chain connectors could direct zeolite formation away from lamellar (2D) to tubular (1D) materials and allow the formation of a cylindrical zeolitic wall.

The formation of nanotubes was apparent from transmission electron microscopy (TEM) images showing individual nanotubes and nanotube bundles in the as-made material (fig. S2, A and B) and after SDA removal by calcination at 823 K (Fig. 2A and fig. S2, C and D). Other materials such as 3D crystals or 2D nanosheets were not observed. The typical nanotube yield (see the materials and methods) was >28% based on Si and >60% based on Al. High-resolution N_2 physisorption at 77 K (24) clearly revealed mesopores (the nanotube channels that form the bulk of the total porosity) and micropores (indicating zeolitic nanotube walls) (fig. S3). The mesopore size distribution (BJH method) shows a narrow peak at ~2.5 nm, suggesting a quite monodisperse channel diameter. The micropore size distribution (HK method) shows a peak at ~0.5 nm in the range of a medium-pore zeolite. Because of the large mesoporosity, the nanotubes have a very high BET surface area of 980 m²/g compared with 410 m²/g for a conventional MFI material. Ar adsorption measurements (fig. S4, A and B) allow greater microporosity resolution. The mesopore size distribution (fig. S4C) exhibits a sharp peak at 3 nm, in good agreement with N2 physisorption. The micropore size is in the same range (5.6 to 6.2 Å) as those of conventional MFI and beta zeolites (fig. S4D). An artifact peak at 8 to 12 Å in all three materials is caused by a known phase transition of adsorbed Ar (7).

Low-angle and wide-angle powder x-ray diffraction (PXRD) patterns of the calcined nanotubes are shown in Fig. 2, B and C (also see fig. S5). As shown earlier for imogolite nanotubes (25, 26), the low-angle PXRD patterns are dominated by the scattering form factors of individual nanotubes and small nanotube bundles, and the primary peak position approximately corresponds to the outer diameter of individual nanotubes. This peak (~4.2 nm in Fig. 2B) is representative of the nanotube diameter, and the subsequent peaks (2 and 1.1 nm) are higher-order scattering peaks. The peaks (0.58 and 0.39 nm) in the wide-angle PXRD pattern indicate periodicity within the nanotube walls (Fig. 2C). The curvature of thin (~1-nm) nanotube walls into a closed cylinder rather than an extended 3D crystal or 2D sheet results in broad PXRD peaks unsuited for structure determination (27-29). Figure S6A shows the Fourier transform infrared (FTIR) spectra of the as-made and calcined nanotubes and the pure SDA. Peaks from the SDA are visible in as-made nanotubes and disappear upon calcination. Peaks in the ~1225 and ~550 cm⁻¹ regions are clearly present in the nanotubes and indicate pentasil [silicate five-membered rings (5MRs)] structural units (30-33). Figure

Fig. 1. Structure-directing agent BCPh10Qui-1,1'- (([1,1'-biphenyl]-4,4'-diylbis(oxy))bis(decane-10,1-diyl))bis(quinuclidin-1-ium) bromide.

S6B compares the FTIR spectra of calcined nanotubes with three pentasil-rich zeolites: 3D BEA, 3D MFI, and 2D MFI. The BEA and MFI spectra show well-known and distinct 5MR signatures at ~1225 cm⁻¹ (external asymmetric stretching of 5MR chains) and 525 to 580 cm⁻¹ (double 5MRs) (30-34). The ²⁹Si nuclear magnetic resonance (NMR) spectrum of the asmade nanotubes (fig. S7A) shows three peaks at -99 ppm (Q³), -106.6 ppm (Q⁴ 3Si,1Al), and -113.3 ppm (Q⁴ 4Si). The Q³ signals are from Si atoms on the wall surface that are presumably terminated by Si-OH groups, and Q⁴ signals are from interior Si atoms in the wall. The Al-bonding environment (27Al NMR peak at 54 ppm; fig. S8) in as-made and calcined nanotubes corresponds to tetrahedral Al, with no evidence of octahedral or extraframework Al. On the basis of the peak areas (35), the Si/ Al ratio was calculated as 16. The fraction of Q³ Si atoms is 0.15, similar to 2D zeolite sheets with nearly single-unit cell thicknesses (36, 37).

¹School of Chemical & Biomolecular Engineering, Georgia Institute of Technology, Atlanta, GA 30332, USA. ²Department of Materials and Environmental Chemistry, Stockholm University, 10691 Stockholm, Sweden. ³School of Chemistry and Biochemistry, Georgia Institute of Technology Atlanta, GA 30332, USA. ⁴Department of Chemical Engineering, The Pennsylvania State University, University Park, PA 16802, USA.

^{*}Corresponding author. Email: sankar.nair@chbe.gatech.edu (S.N.); cjones@chbe.gatech.edu (C.W.J.); tom.willhammar@mmk.su.se (T.W.)

The calcined nanotubes (fig. S7B) show peaks at $-102 \text{ ppm } (Q^3) \text{ and } -110 \text{ ppm } (Q^4), \text{ with a } Q^3$ fraction of 0.17. This value is similar to the asmade nanotubes and indicates no significant condensation of surface silanols after calcination. Normalized FTIR spectra for the nanotubes and a beta zeolite of similar Si/Al ratio (fig. S9) show a similar nature of silanol peaks in both materials, with higher silanol peak intensity in the nanotubes. Isolated (3745 cm⁻¹), terminal (3710 cm⁻¹), internal (3670 cm⁻¹), Albridged (3610 cm⁻¹), and H-bonded (3520 cm⁻¹) silanols (38, 39) are recognizable, but the presence of multiple broad O-H stretch bands at lower wave numbers precludes the identification of any other peaks (40).

The acid site densities were estimated by temperature-programmed desorption of ammonia (NH3-TPD) and FTIR measurements of pyridine adsorption on the nanotubes in their proton-exchanged form. Figure S10A shows NH₃-TPD traces and acid site concentrations for the proton-exchanged nanotubes and, for comparison, a conventional MFI (ZSM-5) catalyst with a similar Si/Al ratio (20). The strength and density of weak acid sites for the two materials are quite comparable, but ZSM-5 has more strong acid sites. The ZSM-5 catalyst would have a theoretical acid site density of 794 µmol/g, close to the measured sum of weak and strong acid sites (721 µmol/g) shown in fig. S10A. The nanotubes have a measured total acid site density of 479 µmol/g (the theoretical value is 988 µmol/g based on the Al content). The sum of Brønsted (B) and Lewis (L) acid site densities measured by pyridine adsorption is 151 µmol/g (fig. S10B), much lower than the NH₃-TPD result. The nanotube material thus has an acid site accessibility factor (AF = pyridine acid site density/NH3 acid site density) of 0.31 and a B/L site ratio of 0.93. Although ²⁷Al NMR provides no evidence for extraframework Al (fig. S8) that is sometimes hypothesized to provide Lewis acid sites, it has been shown (41) that there is no correlation between such Al sites and Lewis acid site densities in zeolites. The moderate AF may relate to the high aggregation tendency of the nanotubes, making a considerable fraction of acid sites inaccessible to the larger pyridine molecules. Discrepancies between NH3-TPD and pyridine infrared are well known in zeolites and other materials (42, 43), but detailed analvsis of the nanotube acid site behavior should be performed in the future.

The crystal structures of most polycrystalline 3D periodic zeolites have been determined either from 3D electron diffraction or PXRD. For materials lacking 3D periodicity, such as 2D zeolites, high-resolution TEM imaging has been key to structure elucidation. These techniques are particularly challenging in the present context because of the reduction of the zeolite to a hollow cylindrical 1D form with a

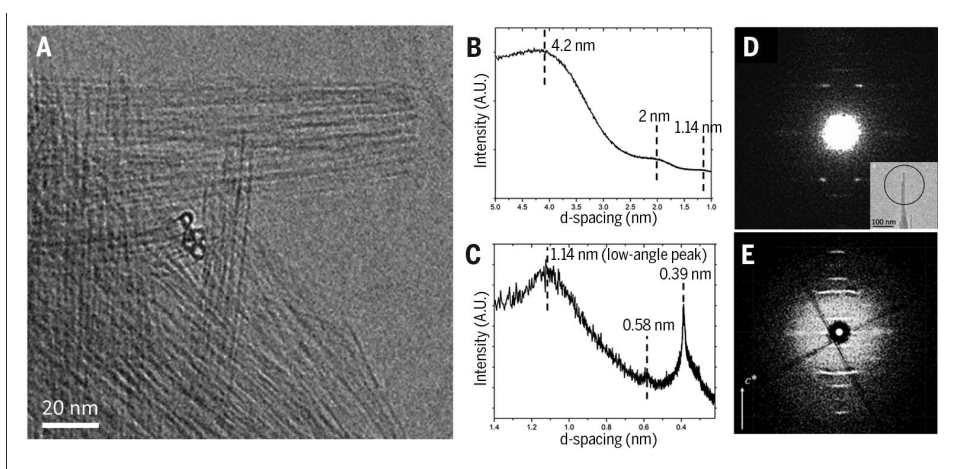
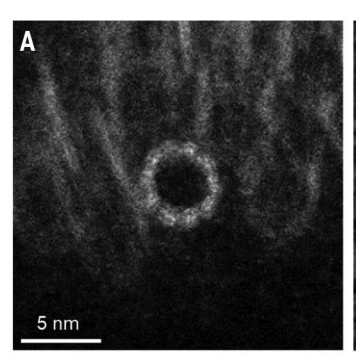


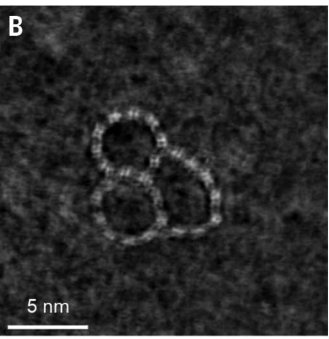
Fig. 2. Zeolite nanotube morphology and diffraction patterns. (A) TEM image showing the tubular morphology of the calcined zeolitic nanotube material. (B and C) PXRD patterns of the calcined nanotube material showing low-angle (B) and wide-angle (C) regions. (D) Selected area electron diffraction pattern from a nanotube (marked in the inset) showing typical tubular features with periodicity along the nanotube direction and characteristic diffraction streaks perpendicular to the nanotube direction. (E) Reconstructed 3D reciprocal lattice from cRED data collected from a bundle of zeolitic nanotubes with the nanotube direction c^* marked.

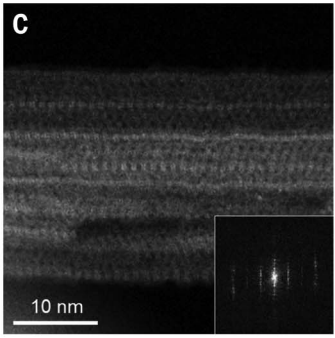
very thin (~1-nm) wall. A region of the sample consisting of one or two aligned nanotubes was used for selected area electron diffraction (SAED) and 3D continuous rotation electron diffraction (cRED) (Fig. 2, D and E). The patterns show characteristic features similar to those of carbon nanotubes (44) and imogolite nanotubes (45). Both the SAED pattern and reconstructed 3D reciprocal space based on cRED data in Fig. 2, D and E, reveal a distinct periodicity of 12.5 Å along the nanotube direction (denoted c^*), with no apparent periodicity observed perpendicular to the c^* axis.

High-resolution annular dark-field scanning TEM (ADF-STEM) and integrated differential phase contrast (iDPC) images were obtained both perpendicular to and along the nanotube direction after sectioning the nanotubes by ultramicrotomy (Fig. 3). Images acquired along the nanotube direction of individual and fused nanotubes (Fig. 3, A and B, and fig. S11) confirm a tubular structure with an ~5-nm outer diameter and an ~3-nm inner diameter. Ten identical repeating units with square-like features are frequently observed around the circumference of the nanotubes, and the distance between adjacent units is 12 to 13 Å. Occasionally, nanodomains with micropores of ~6-Å diameter and an arrangement resembling 3D zeolite beta (*BEA) (27) are observed (figs. S12 and S13, A to E). The square-like feature is found in both the nanotubes and the zeolite beta-like domains. A structural model of the circumferential building unit of the nanotube (fig. S13E) could be deduced from the image of an incomplete nanotube (fig. S13, A to C) and the beta structure. Images acquired perpendicular to the nanotube direction reveal the projected wall structure in more detail (Fig. 3, C and D). The Fourier transform of the image (inset in Fig. 3C) confirms the periodicity of ~12.5 Å along the nanotube direction and a lack of long-range periodicity perpendicular to the nanotube direction, consistent with the electron diffraction data. Isolated dark features of ~6-Å diameter are observed on the nanotube wall surface (Fig. 3D), revealing the presence of micropores on the nanotube wall. The pore size range corresponds to 10MRs to 12MRs perforating the wall. The micropores are arranged at an oblique angle of ~108° (fig. S14) with respect to the nanotube channel axis at a distance of 12 Å, similar to that in zeolite beta.

On the basis of the iDPC STEM images and the axial periodicity from cRED, the structural model of the nanotube is deduced (Fig. 4). The circumferential building unit (Fig. 3 and fig. S13) is depicted in fig. S15A. Repetition of 10 such building units leads to the circumferential cross-section of the nanotube (Fig. 3A and fig. S15B). In the nanotube circumference, these building units are connected through a 5MR (figs. S13 and S15) rather than through a 6MR as in zeolite beta. Although the connection through a 6MR in zeolite beta retains the orientation of the building units, the connection through a 5MR in the nanotube enforces a ~36° rotation of the building unit relative to its neighbors (fig. S15, B and C). This leads to closure of the cylindrical sheet (nanotube) with 10 building units (fig. S15B). The terminal T sites in the walls can act as branching points to form fused nanotubes. Branching occurs between two circumferential building units, as observed in the ADF and iDPC-STEM images (Fig. 3B and fig. S16). The Q³ fraction of T atoms in the structural model is 0.23, which







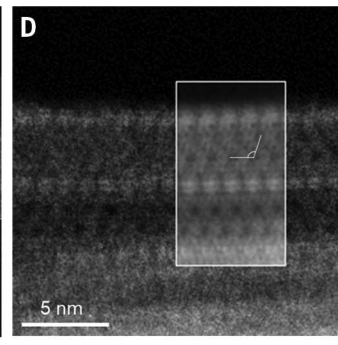


Fig. 3. Zeolite nanotube structure. (**A**) ADF-STEM imaging of an individual single-walled zeolitic nanotube viewed along the nanotube direction. (**B**) Three fused nanotubes imaged with iDPC STEM imaging. The two circular nanotubes (left) each display 10 identical building units around the circumference, and the third tube (right) contains 11 such building units and is no longer circular. (**C**) ADF-STEM image

viewed perpendicular to the nanotube direction, with the Fourier transform (inset) showing a periodicity of 12.5 Å along the nanotube direction. (**D**) enlarged ADF-STEM image revealing the fine structure of the nanotube, with the Fourier-filtered image shown in the inset. Micropores with a diameter of ~6 Å are visible as isolated dark features in (C) and (D), corresponding to 10MRs to 12MRs.

is slightly higher than the value of 0.17 obtained by 29 Si NMR for calcined nanotubes. The branching of the nanotubes and presence of zeolite beta-like nanoregions will reduce the Q^3 fraction of T atoms, leading to a lower Q^3 fraction compared with the ideal nanotube model. The pentasil-rich structure is consistent with the FTIR spectra (fig. S6), showing characteristic 5MR vibrations.

Geometrical optimization of the pure-silica (no Al) nanotube structure was performed after termination of the Q³ Si atoms with hydroxyl groups. The model (Fig. 4, A and B, and structural model in the supplementary materials) converged to a structure with reasonable bond geometries (table S1). The geometryoptimized structure has a periodicity of 12.65 Å along the nanotube axis, which agrees well with the SAED, ADF, and iDPC results. Its outer diameter (based on the outermost Si atoms) and wall thickness are 4.6 and 0.5 nm, respectively, in agreement with the STEM images (fig. S16). The wall structure allows for polytypic structural disorder (fig. S17) similar to 3D zeolite beta (46, 47). This stacking disorder is based on allowed $\pm 1/3$ translations of the 12.65-Å periodicity along the extended c axis. To close the nanotube, the sum of all translation vectors should be an integer $(\pm n^*c)$. This restriction might account for the observation of some incomplete nanotubes in the microscope images. The simulated and experimental PXRD patterns of the individual nanotubes are in very good agreement (fig. S18). A notable feature emerging naturally from the arrangement of the building units is the presence of 10MR and 12MR micropores on the inner and outer wall surfaces, respectively (Fig. 4, C to E). Because of the nanotube curvature, the two surfaces have different topological structures. The outer surface is built from 4MRs, 5MRs, and 6MRs, leading to 12MR micropores, whereas the inner surface is built from only 5MRs and 6MRs, leading to 10MR micropores. The outer surface is topologically identical to a layer of zeolite beta. For the case of strictly consecutive stacking (+1/3, +1/3... or -1/3, -1/3... translations), the inner surface is topologically identical to a building layer in the *ac* plane of zeolite MFI. The nanotube wall can thus be considered a unique "atomic-scale" hybrid of zeolites beta (polymorph B) and MFI. Such a hybrid cannot be formed in a 3D or 2D structure, and instead requires curvature into a cylindrical nanotubular morphology.

To study the energetics of the nanotube diameter, structural models were constructed from six, eight, 10, 12, and 14 building units (fig. S19) and geometrically optimized. The nanotube built from 10 units (which is also the experimentally observed nanotube) has the most favorable geometry in terms of Si-O distances as well as O-Si-O and Si-O-Si angles (table S1 and fig. S20). This nanotube also exhibits a clear minimum in the computed surface energy (fig. S21) caused by optimal balance of bond geometries in the inner and outer surfaces. Because of the curvature-induced strain, the major and minor dimensions of the 12MRs $(7.91 \times 6.44 \text{ Å}, \text{ after subtraction of two oxygen})$ radii of 1.35 Å) and 10MRs (5.89 \times 5.63 Å) in the optimized nanotube structure are distorted relative to the 12MRs in the 3D *BEA [100] proiection $(7.17 \times 6.33 \text{ Å})$ and MFI $(6.23 \times 4.98 \text{ Å})$ optimized with the same force field. This may also influence the effective pore size distributions obtained from Ar adsorption (fig. S4).

To obtain initial observations of the nanotube formation process, synthesis products from 1 to 7 days of hydrothermal synthesis at 423 K were analyzed by PXRD and TEM (figs. S22 and S23). Small-angle PXRD patterns show early development of mesopore domains with a characteristic scale that does not change significantly with time. The wide-angle PXRD patterns show evolution of the nanotube wall structure from amorphous to an ordered zeolitic form. These observations are consistent

with the TEM images, in which the mesoporosity of the material is clearly visible at an early stage. Proto-nanotubes are visible at 3 days and distinct nanotubes at 5 to 7 days. Thus, the overall growth mechanism of the zeolite nanotubes appears to have some similarities to the growth of 2D zeolite nanosheets, i.e., the initial formation of a mesophase followed by transformation to an ordered zeolitic material (48). A key difference is in the morphologydirecting effect of the bolaform SDA used in this work, which creates a 1D nanotubular morphology rather than 2D nanosheets. Other bolaform molecules with aromatic rings in their hydrophobic core are known to π -stack and form stable cylindrical or rod-like micellar assemblies (15, 16, 18-20, 49). Thus, we hypothesized that our bolaform SDA (BCPh10Qui) might π -stack sufficiently to direct the formation of nanotubular zeolites. Figure S24 shows ultraviolet-visible diffuse reflectance absorption spectra of the solid SDA, dilute aqueous SDA solution, and as-made nanotubes. In the dilute solution, the SDA molecules are isolated, and a single absorption is observed at 265 nm (π -HOMO $\rightarrow \pi^*$ -LUMO transition). In the solid SDA, this transition is red-shifted to a double peak beyond 300 nm because of π stacking. The as-made nanotubes also show a double peak that is evidence of significant π stacking, albeit not as extensive as in the solid SDA. Figure S25 compares ¹³C CPMAS NMR spectra of as-made nanotubes and solid SDA and confirms that the SDA is intact in the nanotubes. Elemental analysis (table S2) reveals a C/N atomic ratio of 25 in the as-made nanotubes (agreeing with C/N = 23 in the SDA; Fig. 1) and an Si/Al ratio of 15 (in agreement with the Si/Al ratio of 16 from NMR). Thermogravimetric analysis of the as-made nanotubes shows that the SDA accounts for 51% of total mass (fig. S26), in agreement with elemental analysis in which C, H, and N account for 48% of total mass. The

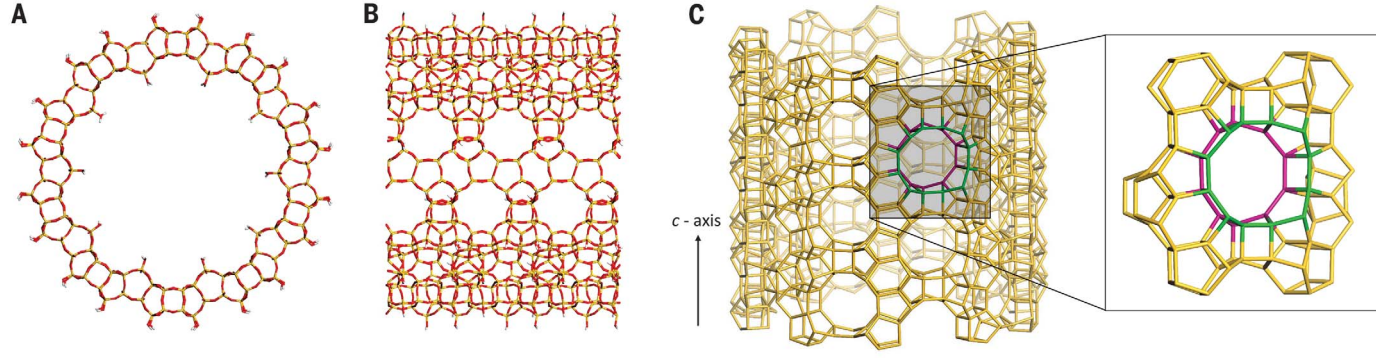
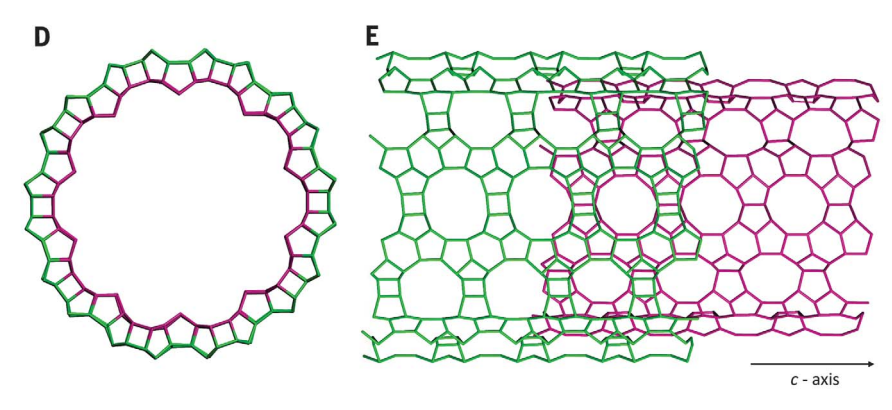


Fig. 4. Zeolite nanotube structural model. (A and

B) Geometry-optimized structure viewed along (A) and perpendicular to (B) the nanotube channel axis (defined as the c axis). The T (T = Si/AI) atoms are shown in yellow, oxygen in red, and hydrogen in white. The building unit is extracted from the structure of zeolite beta. (C) The nanotube inner wall surface has 10MR micropores like zeolite MFI, and the outer wall surface has 12MR micropores similar to zeolite beta (code BEA). (**D**) Composite view of inner (purple) and outer (green) wall surfaces along the nanotube axis. (E) Separated views of the inner (purple) and outer (green) wall surfaces perpendicular to the nanotube axis. The outer surface is topologically identical to a projection of zeolite beta (in this case, polymorph B) and the inner surface to a projection of zeolite MFI.



hydrophobic core of the long-chain SDA is the main contributor to this high organic content, which is also seen in hierarchical 2D zeolitic materials synthesized with long-chain SDAs (14, 15, 19, 20),

In conclusion, a quasi-1D zeolite in the form of single-walled nanotubes with zeolitic walls has been synthesized for the first time and its structure revealed. The concept of directing zeolite nanotube synthesis using bolaform SDAs capable of π -stacking of the hydrocarbon core is introduced. Closure of a thin zeolitic sheet into a nanotube is shown to result in a nanotube wall with structurally different inner and outer surfaces, in the present case, a hybrid of zeolite beta and MFI layers. The exact arrangement of the SDA molecules in the asmade nanotubes is not currently known. Our experimental observations suggest that the biphenyl rings of the SDA molecules may form a stable π -stacked hydrophobic core along the nanotube axis, whereas the flexible alkyl chains with the quinuclidinium head groups stretch out along the radius of the nanotube in different directions, reaching into the microporous walls that are templated by the head groups. A number of different 1D zeolite nanotubes could potentially be synthesized by the above concept using a wide range of bolaform SDAs and reaction conditions. More detailed studies of the formation mechanisms and the effects of synthesis conditions are also

desirable to better guide such strategies. The zeolitic nanotubes are stable under hightemperature calcination, like 2D and 3D zeolites. New functional properties could result from the ability to transport molecules axially within catalytically active nanotubular zeolitic channels while also allowing radial molecular transport, exchange, and catalytic conversion through the ultrathin (~1-nm) microporous wall. These phenomena cannot be realized with conventional nanotubes.

REFERENCES AND NOTES

- 1. C. S. Cundy, P. A. Cox, Chem. Rev. 103, 663-702 (2003).
- A. Corma, J. Catal. 216, 298-312 (2003).
- M F Davis Nature 417 813-821 (2002)
- Y. Tao, H. Kanoh, L. Abrams, K. Kaneko, Chem. Rev. 106, 896-910 (2006).
- J. Čejka, S. Mintova, Catal. Rev., Sci. Eng. 49, 457-509 (2007).
- X. Zhang et al., Science 336, 1684-1687 (2012).
- K. Na et al., Science 333, 328-332 (2011).
- V. J. Margarit, M. F. Martínez-Armero, M. T. Navarro, C. Martínez. A. Corma, Angew. Chem. Int. Ed. 54, 13724-13728 (2015).
- K. Möller, T. Bein, Chem. Soc. Rev. 42, 3689-3707 (2013).
- 10. D. Verboekend, J. Pérez-Ramírez, Catal. Sci. Technol. 1,
- 11. R. A. Beyerlein, C. Choi-feng, J. B. Hall, B. J. Huggins, G. J. Ray, Top. Catal. 4, 27-42 (1997).
- 12. A. Feliczak-Guzik, Microporous Mesoporous Mater. 259, 33-45 (2018)
- 13. W. Fan et al., Nat. Mater. 7, 984-991 (2008).
- 14. M. Choi et al., Nature 461, 246-249 (2009).
- 15. D. Xu et al., Nat. Commun. 5, 4262 (2014).
- 16. D. Xu, Z. Jing, F. Cao, H. Sun, S. Che, Chem. Mater. 26. 4612-4619 (2014).
- 17. D. P. Serrano, J. M. Escola, P. Pizarro, Chem. Soc. Rev. 42, 4004-4035 (2013).
- 18. B. K. Singh et al., Chem. Mater. 26, 7183-7188 (2014).

- 19. X. Shen et al., Angew. Chem. Int. Ed. 57, 724-728 (2018).
- 20. Y. Zhang et al., Chemistry 25, 738-742 (2019).
- 21. Y. Zhang, Y. Ma, S. Che, Chem. Mater. 30, 1839-1843 (2018).22. Y. Zhang, S. Che, Angew. Chem. Int. Ed. 59, 50-60 (2020).
- 23. Y. Seo, S. Lee, C. Jo. R. Rvoo, J. Am. Chem. Soc. 135.
- 8806-8809 (2013).
- 24. P. I. Ravikovitch, S. C. O. Domhnaill, A. V. Neimark, F. Schiith, K. K. Unger, Langmuir 11, 4765-4772 (1995).
- 25. D. Y. Kang et al., Nat. Commun. 5, 3342 (2014)
- 26. D. Y. Kang et al., ACS Nano 4, 4897-4907 (2010).
- 27. Database of Zeolite Structures, http://www.iza-structure.org/ databases/
- 28. R. Pophale, P. A. Cheeseman, M. W. Deem, Phys. Chem. Chem. Phys. 13, 12407-12412 (2011).
- 29. O. Knio, A. J. Medford, S. Nair, D. S. Sholl, Chem. Mater. 31, 353-364 (2019).
- 30. J. C. Jansen, F. J. van der Gaag, H. van Bekkum, Zeolites 4, 369-372 (1984).
- 31. G. Coudurier, C. Naccache, J. C. Vedrine, J. Chem. Soc. Chem. Commun. (24): 1413-1415 (1982).
- 32. P. A. Jacobs, H. K. Beyer, J. Valyon, Zeolites 1, 161-168
- 33. D. Lesthaeghe et al., J. Phys. Chem. C 112, 9186-9191 (2008).
- 34. S. R. Tomlinson, T. McGown, J. R. Schlup, J. L. Anthony, Int. J. Spectrosc. 2013, 1-7 (2013).
- 35. J. Klinowski, S. Ramdas, J. M. Thomas, C. A. Fyfe, J. S. Hartman, J. Chem. Soc. Faraday Trans. 2 Mol. Chem. Phys. **78**. 1025-1050 (1982).
- 36. H. Zhang et al., Angew. Chem. Int. Ed. 55, 7184-7187 (2016).
- 37. J. E. Schmidt, D. Xie, M. E. Davis, Chem. Sci. 6, 5955-5963 (2015).
- 38. J.-P. Gallas et al., Langmuir 25, 5825-5834 (2009).
- 39. A. A. Gabrienko et al., J. Phys. Chem. C 122, 25386-25395 (2018).
- 40. F. Eder, M. Stockenhuber, J. A. Lercher, J. Phys. Chem. B 101, 5414-5419 (1997).
- 41. M. Ravi, V. L. Sushkevich, J. A. van Bokhoven, Nat. Mater. 19. 1047-1056 (2020).
- 42. P. M. Kester, J. T. Miller, R. Gounder, Ind. Eng. Chem. Res. 57, 6673-6683 (2018).

- 43. J. S. Yoon, M. B. Park, Y. Kim, D. W. Hwang, H.-J. Chae, Catalysts 9, 933 (2019).
- 44. J. C. Meyer, M. Paillet, G. S. Duesberg, S. Roth, Ultramicroscopy **106**, 176-190 (2006).
- 45. P. D. G. Cradwick et al., Nat. Phys. Sci (Lond.) 240, 187-189 (1972).
- 46. M. M. J. Treacy, J. M. Newsam, Nature 332, 249-251
- (1988). 47. F. Taborda, T. Willhammar, Z. Wang, C. Montes, X. Zou, Microporous Mesoporous Mater. 143, 196-205 (2011). 48. K. Na et al., J. Am. Chem. Soc. 132, 4169-4177 (2010).
- 49. C. Wang, Z. Wang, X. Zhang, Acc. Chem. Res. 45, 608-618
- (2012).

ACKNOWLEDGMENTS

Funding: This work was supported by the National Science Foundation (grant no. CBET-1534179 to S.N., C.W.J., D.S.S., A.K., B.M., and O.K.) and the Swedish Research Council (grant no. 2017-04321 to

X. Zou and grant no. 2019-05465 to T.W.). PXRD and SEM characterizations were performed at the Georgia Tech Institute for Electronics and Nanotechnology, home to one of the 16 sites of the National Nanotechnology Coordinated Infrastructure (NNCI), which is supported by the National Science Foundation (grant no. ECCS-1542174). Materials characterization at Penn State University was performed at the Materials Characterization Laboratory, which is a partner in the National Nanotechnology Infrastructure Network (NNIN) and the Materials Research Facilities Network (MRFN), supported by the US National Science Foundation (award no. DMR-1420620). Author contributions: A.K., B.M., C.W.J., and S.N. conceived this work. A.K., B.M., I.N., Z.W., J.L., X.Y., and X. Zhang performed nanotube synthesis and initial structure characterization. E.K., X. Zou, and T.W. performed detailed structure determination. O.K., D.S.S., and T.W. performed model calculations. All authors participated in the interpretation of data and writing of the manuscript. **Competing interests:** A patent application (PCT/US21/44710) titled "Zeolite Nanotubes and Methods of

Making and Use Thereof" (inventors: S.N., C.W.J., A.K., J.L., B.M., and Z.W.; applicant: Georgia Tech Research Corporation) was filed on 5 August 2021 and claims priority over our earlier US provisional application 63/061,449 filed on 5 August 2020. Data and materials availability: All data are available, either in numerical or graphical form, in the main text or the supplementary materials.

SUPPLEMENTARY MATERIALS

science.org/doi/10.1126/science.abg3793 Materials and Methods Tables S1 and S2 Figs. S1 to S26 References (50-61) Structural Model (CIF File)

31 December 2020; accepted 5 November 2021 10.1126/science.abg3793

5 of 5 Korde et al., Science 375, 62-66 (2022) 7 January 2022



Single-walled zeolitic nanotubes

Akshay KordeByunghyun MinElina KapacaOmar Kniolman NezamZiyuan WangJohannes LeisenXinyang YinXueyi ZhangDavid S. ShollXiaodong ZouTom WillhammarChristopher W. JonesSankar Nair

Science, 375 (6576), • DOI: 10.1126/science.abg3793

Zeolitic nanotubes

Nanotubes generally have solid walls, but a low-dimensional version of zeolites now introduces porosity into such structures. Korde *et al.* used a structure-directing agent with a hydrophobic biphenyl group center connecting two long alkyl chains bearing hydrophilic bulky quaternary ammonium head groups to direct hydrothermal synthesis with silicon-rich precursors (see the Perspective by Fan and Dong). The nanotubes have a mesoporous central channel of approximately 3 nanometers and zeolitic walls with micropores less than 0.6 nanometers. Electron microscopy and modeling showed that the outer surface is a projection of a large-pore zeolite and the inner surface is a projection of a medium-pore zeolite. —PDS

View the article online

https://www.science.org/doi/10.1126/science.abg3793

Permissions

https://www.science.org/help/reprints-and-permissions

Use of this article is subject to the Terms of service